# Bending-Induced Enhancement of Longitudinal Optical Phonon Scattering in ZnO Nanowires

**Fang Fang,*,† Dongxu Zhao,*,‡ Binghui Li,‡ Zhenzhong Zhang,‡ Dezhen Shen,‡ and Xiaohua Wang†**

*Changchun University of Science and Technology, 7089 Wei-Xing Road, Changchun 130022, People's Republic of China, and Key Laboratory of Excited State Processes, Changchun Institute of Optics, Fine Mechanics and Physics, Chinese Academy of Sciences, 16 East Nan-Hu Road, Open Economic Zone, Changchun 130033, People's Republic of China*

*Received: April 27, 2010; Revised Manuscript Received: June 19, 2010*

The coupling of piezoelectric and semiconducting properties in zinc oxide created a strain field and charge separation across the nanowire as a result of its bending. Such built-in fields open an additional channel of electron−phonon coupling that enhanced the longitudinal optical phonons scattering significantly.

On the basis of the remarkable physical properties of nanoscale zinc oxide, such as semiconducting, piezoelectric (PZ), mechanical, and biocompatible properties, much effort has been invested in the synthesis, characterization, and device applications of ZnO nanomaterials in recent years. A variety of functional devices based on ZnO nanostructures, such as gas and chemical sensors, ultraviolet lasers, light-emitting diodes (LEDs), photodetectors, and piezoelectric nanogenerators, have been fabricated.[1–6]

Fabrication of efficient devices based on ZnO nanostructures, such as LEDs, requires in-depth understanding of the luminescent and electric properties of the nanostructures under different conditions. We notice that the bending and bundling are a common phenomenon of ZnO nanostructures, especially for the hydrothermally grown ZnO nanowires. Besides the bending during the growth, they also have a high possibility of bending deformation in the course of nanodevice design and fabrication. Because of the existence of piezoelectric field in bended ZnO nanowires, they may have different properties compared with the straight ones. But few reports concern the effect of bending on the Raman and photoluminescence (PL) properties of ZnO nanowires. There are two main reasons: First, some bending phenomenon often occurs during the growth.[7–10]Second, current nanomechanical bending experiments are all based on the in situ SEM/AFM/TEM.[11–13] Therefore, measurements without the participation of those microscopes cannot be realized.

In this paper, the bended ZnO nanowires were obtained by a polymer coating process. We analyzed the changes of PL and Raman spectra before and after bending. In our experiment, when the ZnO nanowire (NW) arrays contact polymer, the whole array bended in large scale. Here, on one hand, such a polymer driven method can avoid the above requirement for such measurement effectively; on the other hand, polymer and organic solvent are usually used in the course of nanodevice fabrication. For example, the polymer is filled in the space of ZnO NW arrays for LED application and organic dye is used in NW-based dye-sensitized solar cells.[14,15] In these processes, the bending is inevitable. Most interestingly, an enhancement of longitudinal optical (LO) phonon scattering is observed in both PL and Raman spectra as a result of its bending. A possible mechanism, which by combining the PZ and semiconducting properties in zinc oxide creating a built-in field in the bended NWs can strongly modulate the LO phonon modes, was addressed.

The ZnO NWs used in our experiments are fabricated via a simple vapor-phase transport process on Si (001) substrate in a horizontal tube furnace described previously.[16] Field-emission scanning electron microscopy (FESEM) (Figure 1a) shows that the as-grown NWs are well-aligned along the normal direction of the substrate. The as-grown sample is vertically oriented and uniform NWs with diameters $d = 100$ to 200 nm, heights $h = 10$ to 13 $\mu$m, aspect ratios $h/d = 50$ to 130. The inset of Figure 1a shows an amplified top image of a single NW, which indicates the top of NW is flat with a hexagonal shape. The energy-disperse X-ray (EDX) attached to the SEM analysis also indicates that there are zinc and oxygen elements on the ZnO NWs (atom % Zn:O = 3:2) (Figure 1b).

The poly(*N*-vinylcarbazole) (PVK) powder is sonicated in chloroform for 1 h at room temperature with concentrations of 10 mg/mL. By dripping the polymer solution on the surface of the NW arrays, the vertically aligned ZnO NWs are bended during the solvent-evaporation process. The morphology of NWs with PVK is shown in Figure 1c. The SEM images reveal that the adjacent NWs attach together due to polymer shrinkage. The compressive residual stresses resulting from polymer shrinkage transfer to the NWs via a polymer cohesion process, which leads to the bending of NWs. Here, the image of the NWs becomes difficult due to the presence of the polymer.[17] To minimize the negative effect, the sample is rinsed by pure chloroform solvent to dissolve the PVK residues. As shown in Figure 1d, the morphology of the sample does not change after the rinsing process (the inset images shown at high magnification).

Figure 2 shows the X-ray diffraction (XRD) spectra of the as-grown ZnO NWs and bended ZnO NWs. Both samples are *c*-axis preferred orientation, which can be confirmed by only the ZnO (002) diffractive peak appearing in the spectra. In contrast to the as-grown ZnO NWs, the bended NWs have a weaker intensity of the (002) diffractive peak. Obviously, the

* To whom correspondence should be addressed. Phone: +86-431-86176322. Fax: +86-431-4627031. E-mail: fangfang1982131@yahoo.com.cn (F.F.) or dxzhao2000@yahoo.com.cn (D.Z.).
† Changchun University of Science and Technology.
‡ Chinese Academy of Sciences.

10.1021/jp1037975 
Published on Web 07/02/2010

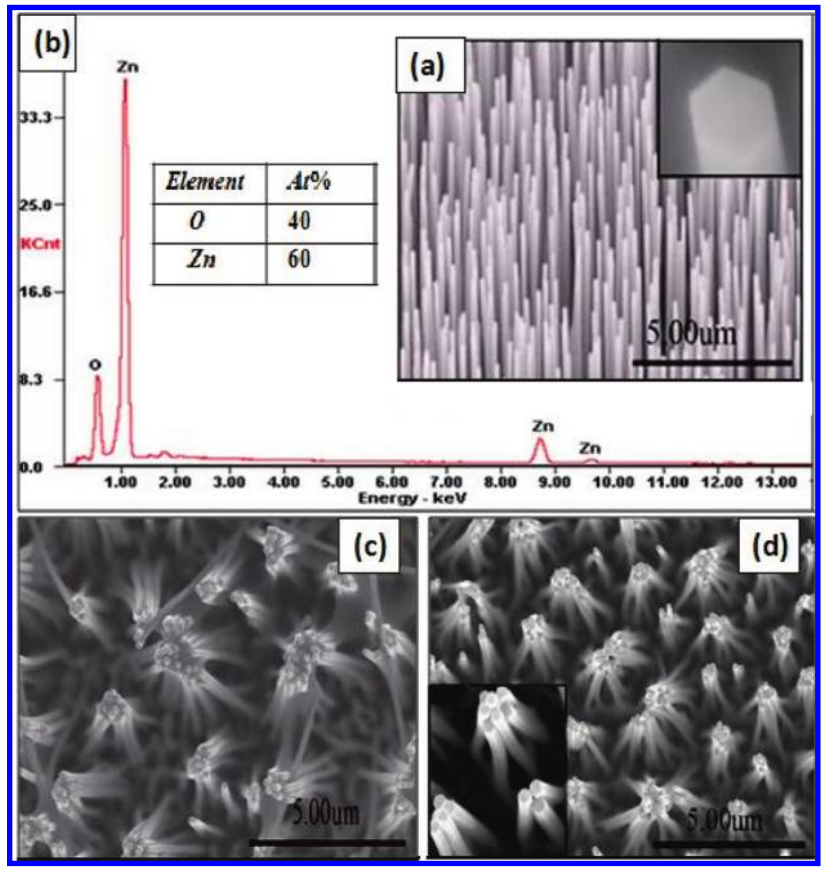


**Figure 1.** (a, b) FESEM images and EDX spectrum of the as-grown ZnO NWs formed on Si substrate. The inset in part a shows the faceted hexagonal shape of the NW. (c) FESEM images of ZnO NW arrays after dripping the macromolecular solution on the surface with 10 mg/mL concentration. (d) ZnO NW arrays after rinsing the PVK residues (the inset images are shown at high magnification).

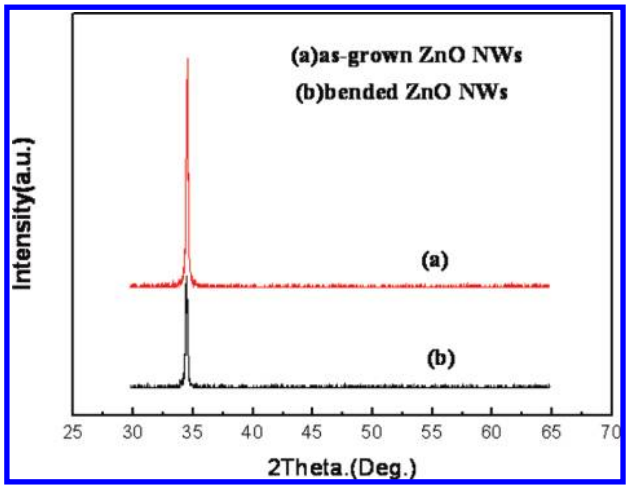


**Figure 2.** XRD results of (a) as-grown ZnO NWs and (b) bended ZnO NWs (the intensity axis is linear).

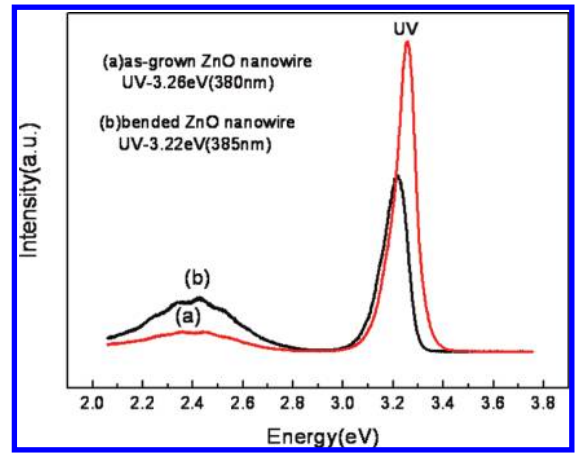


**Figure 3.** Room temperature PL spectrum of (a) as-grown ZnO NWs and (b) bended ZnO NWs (the intensity axis is linear).

PVK treatment deteriorates the well-aligned orientation of as-grown ZnO NWs. Meanwhile, comparing the (002) diffractive peak position of as-grown ZnO NWs ($2\theta = 34.52°$) with the bended one ($2\theta = 34.45°$), the (002) positions have a little deviation. It is suggested that there may be some residual strain in the bended ZnO NWs during the bending deformation.

To study the optical properties, the PL spectrum was measured using a He−Cd laser line of 325 nm as an excitation source. Here, all the positions of the emission peak have been calibrated by the laser line. Figure 3 shows the room temperature PL spectrum. The PL spectra of both samples are composed of two main parts: one is the excitonic emission with energy around the band gap of ZnO in the UV region (as-grown and bended ZnO NWs have two peaks centered at 3.26 eV (380 nm) and 3.22 eV (385 nm), respectively), which is attributed to the near-band-edge exciton emission; the other is the defect-related deep level emission in the visible range. The deep-level emission at around 2.43 eV (510 nm) is commonly believed to come from the singly ionized oxygen vacancy or surface states.[18,19] The deduction is in accordance with the EDX result, which shows stochiometrically less oxygen than zinc in the product (EDX data shown in Figure 1b). In addition, in contrast to the as-grown sample, the band gap PL intensity of bended ZnO NWs decreases. The decrease in band gap PL intensity could be simply due to a sum-rule: the defects generated by bending

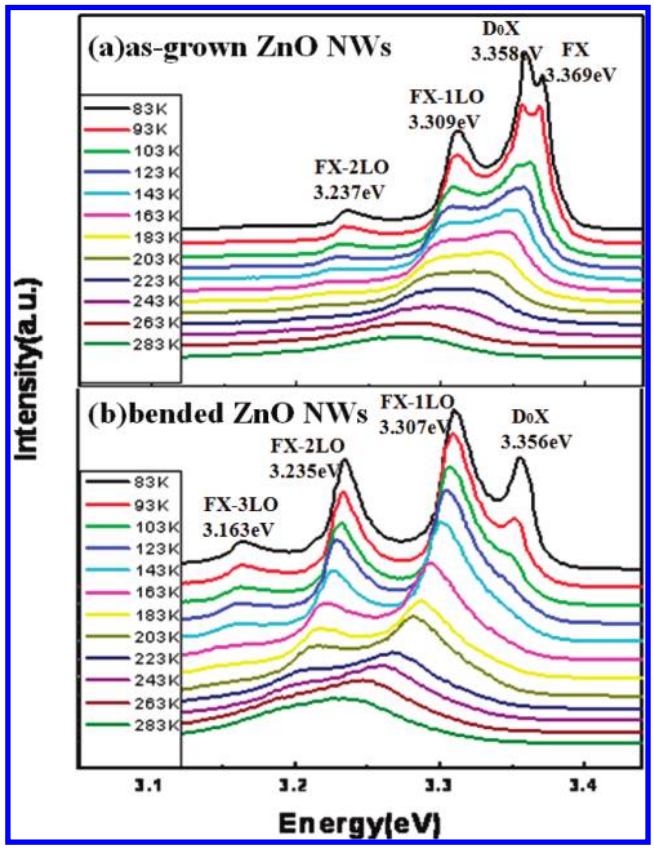


**Figure 4.** PL spectra of the ZnO nanowires measured at different temperatures (from 83 to 283 K): (a) as-grown ZnO NW arrays and (b) bended ZnO NW arrays (the intensity axis is linear).

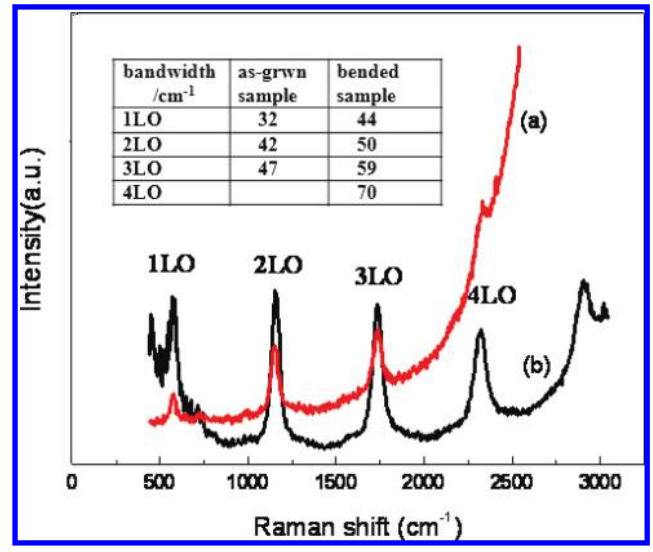


**Figure 5.** Resonance Raman spectra of (a) as-grown ZnO NWs and (b) bended ZnO NWs excited with a He−Cd laser (the intensity axis is linear).

deformation enhanced the emission in the visible range. So, if more recombination is through defects (the ~2.4 eV broad feature), than less should be left for direct-gap recombination.

To analyze the origin of the emission peaks, the PL of two samples have been measured in the temperature range between 83 and 283 K. At 83 K, the PL spectra of as-grown ZnO NWs show various peaks located at 3.369, 3.358, 3.309, and 3.237 eV, respectively, as shown in Figure 4a. The dominant peak at 3.358 eV and its shoulder (at the higher energy) at 3.369 eV can be assigned to a neutral donor bound exciton ($D_0X$) and a free-exciton (FX) emission. At the lower energy position of $D_0X$, two emission peaks emerge, which are considered to be the phonon replicas of FX. Here, the energy separation of FX-1LO is smaller than the LO phonon energy (72 meV) due to the energy softening of FX-1LO.[20] It can be clearly seen that the whole peak position of bended ZnO NWs has a shift to low energy: $D_0X$, from 3.358 to 3.356 eV; FX-1LO, from 3.309 to 3.307 eV; and FX-2LO, from 3.237 to 3.235 eV. The inner and outer surfaced of each bended ZnO NW suffer opposite strains. As we know, compressive strain normally causes a blue shift of PL and tension strain for a red shift. The possibility for this red shift in our experiment could be attributed to the comprehensive effect of tension and compression stains as a result of bending.[21−23] There is a distinct difference for the FX-phonon replicas emission intensity of the two samples. For the as-grown sample, the FX recombination is stronger than its phonon replica at 83 K. While in the spectrum of the bended one, the dominating emission peak is the FX-1LO replica. In addition, the FX-phonon coupling effect is enhanced obviously such that we can see the FX-3LO shown at 3.163 eV in Figure 4b. Such significant variation in FX-phonon coupling between two samples is due to different exciton annihilation processes, i.e., exciton scattering by LO phonons is a particularly efficient luminescence path.[24] The enhanced effect of phonon modes in bended ZnO NWs will be interpreted in the Raman spectrum below. With the increase of temperature, the emission peaks moved toward the lower energy side and gradually became broader due to the LO-phonon scattering and increased exciton thermal ionization,[25] and the exciton-related emissions of bended ZnO nanowires are quenched so fast that they could not be observed at 143 K. This result suggested that UV emission of bended ZnO nanowires mainly originates from FX-LO phonon replicas. For the straight ZnO nanowires the near band-edge emission at room temperature is a dual contribution of FX and FX-LO phonon. Therefore the photon emission peak of bended nanowires shifts to the low energy side at room temperature.

The above low-temperature PL spectra show an enhancement of FX-LO emission for bended ZnO nanowires. To better understand the effect of bending on the phonon vibration, resonance Raman spectra were performed at room temperature. Figure 5 shows Raman scattering spectra for (a) as-grown ZnO NWs and (b) bended ZnO NWs. The first-order LO modes of ZnO resonance Raman peaks are measured to be 570 $cm^{-1}$. Compared to the as-grown sample, the position of the LO mode is nearly maintained unchanged, but bended ZnO NWs have stronger Raman signals. The vibration orders of ZnO resonance Raman peaks are also increased from 4 orders to 5 orders accompanied by bandwidth broadening (as shown in Figure 4).

The built-in electric field in the bended ZnO NWs would be appropriate for understanding this experiment. For a vertical, straight ZnO NW, the deflection of the NW by polymer shrinkage creates a strain field, with the outer surface being stretched and the inner surface compressed. An electric field $E$ along the NW was then created inside the NW volume through the PZ effect.[26] The electric potential was created by the relative displacement of the $Zn^{2+}$ cations with respect to the $O^{2-}$ anions, as a result of the PZ effect in the ZnO wurtzite crystal structure. The most probable route of action of the built-in electric field in the described NWs is through an additional electron−phonon interaction, which enhances the signal associated with the LO phonon. Similar phenomena have been observed in multiple-quantum-well and superlattice structures.[27,28] Such a Raman process is due to Frohlich-interaction electron−phonon scattering activated by the strain-generated electric fields that occur

in the multiple-quantum-well structures. For the wurtzite structure crystals, stress induced in the crystals obviously affected the $E_2$ (high) phonon frequency.[29] In our experiment the weak peak around 437 $cm^{-1}$, which was contributed to the $E_2$ (high) mode, was almost imperceptible in as-grown ZnO NWs compared with other (overlapping/stronger) resonance Raman scattering peaks. However, we could also deduce that strain was present in the ZnO NWs because of the Raman phonon bandwidth broadening.[30]

In conclusion, the effect of bending on PL and Raman spectra in ZnO NWs has been studied in detail. The results suggest that the coupling of PZ and semiconducting properties in zinc oxide created a local electric field after bending, and such built-in fields open an additional channel of electron−phonon coupling that enhanced the signal associated with the LO phonon significantly. Although the Raman intensity of the LO phonon and FX-phonon coupling modes in PL spectra are reinforced, the UV intensity in PL decreases after bending. All of the above results further show that such deformation caused during the fabrication of nanodevices should be paid more attention.

**Acknowledgment.** This work is supported by the Key Project of National Natural Science Foundation of China under Grant No. 50532050, the "973" program under Grant No. 2006CB-604906, the CAS Innovation Program, the National Natural Science Foundation of China under Grant No. 60506014, the Project of Science Development Planing of Jilin Province (20070519, 20090139, 20090555, 20080331-1), the Program for New Century Excellent Talents in University (NCET-07-022), the Project of Science Development Planing of Jilin Province (20070519, 20090139, 20090555, 20080331-1), and the Program for New Century Excellent Talents in University (NCET-07-022).

## References and Notes

(1) Pan, Z. W.; Dai, Z. R.; Wang, Z. L. *Science* **2001**, *291*, 1947.
(2) Park, W. I.; Yi, G. C. *Adv. Mater.* **2004**, 16,87.
(3) Wang, X. L.; Yang, F.; Yang, W.; Yang, X. R. *Chem. Commun.* **2007**, 4419.
(4) Wang, X. D.; Song, J. H.; Wang, Z. L. *J. Mater. Chem.* **2007**, 17,711.
(5) Wang, X. L.; Zhu, H.; Wang, Z. J.; Yang, F.; Yang, X. R. *Chem.—Eur. J.* **2009**, 15,4253.
(6) Cuscó, R.; Alarcón-Lladó, E.; Ibáñez, J.; Artús, L.; Jiménez, J.; Wang, B. G.; Callahan, M. *J. Phys. Rev. B* **2007**, 75,165202.
(7) Lu, C. H.; Limin, Qi.; Yang, J. H.; Li, T.; Zhang, D. Y.; Ma, J. M. *Chem. Commun.* **2006**, 3551.
(8) Sun, Y.; Ndifor-Angwafor, N. D.; George, J.; Ashfold, M. N. R. *Chem. Phys. Lett.* **2006**, *431*, 352.
(9) Sun, Y.; Riley, D. J.; Ashfold, M. N. R. *J. Phys. Chem. B* **2006**, 110,15186.
(10) Lin, Y.-R.; Yang, S.-S.; Tsai, S.-Y.; Hsu, H.-C.; Wu, S.-T.; Chen, I.-C. *Cryst. Growth Des.* **2006**, *6*, 1951.
(11) Wong, E. W.; Sheehan, P. E.; Lieber, C. M. *Science* **1997**, *277*, 1971.
(12) Song, J. H.; Wang, X. D.; Riedo, E.; Wang, Z. L. *Nano Lett.* **2005**, *5*, 1954.
(13) Zhua, C. Q.; Zhua, J. *Appl. Phys. Lett.* **2007**, *90*, 043105.
(14) Law, M.; Greene, L. E.; Johnson, J. C.; Saykally, R.; Yang, P. D. *Nat. Mater.* **2005**, *4*, 455.
(15) Kö nenkamp, R.; Word, R.; Godinez, M. *Nano Lett.* **2005**, *5*, 2005.
(16) Fang, F.; Zhao, D. X.; Zhang, J. Y.; Shen, D. Z.; Lu, Y. M.; Fan, X. W.; Li, B. H.; Wang, X. H. *Nanotechnology* **2007**, *18*, 235604.
(17) Wagner, H. D.; Lourie, O.; Feldman, Y.; Tenne, R. *Appl. Phys. Lett.* **1998**, *72*, 188.
(18) Vanheusden, K.; Warren, W. L.; Sesger, C. H.; Tallant, D. R.; Voigt, J. A.; Gnage, B. E. *J. Appl. Phys.* **1996**, *79*, 7983.
(19) Yao, B. D.; Chan, Y. F.; Wang, N. *Appl. Phys. Lett.* **2002**, *81*, 757.
(20) Liang, W. Y.; Yoffe, A. D. *Phys. Rev. Lett.* **1968**, *20*, 59.
(21) Liu, Z. W.; Ong, C. K.; Yu, T.; Shen, Z. X. *Appl. Phys. Lett.* **2006**, *88*, 053110.
(22) Riaz, M.; Nur, O.; Willander, M.; Klason, P. *Appl. Phys. Lett.* **2008**, *92*, 103118.
(23) Li, Y. F.; Yao, B.; Lu, Y. M.; Cong, C. X.; Zhang, Z. Z.; Gai, Y. Q.; Zheng, C. J.; Li, B. H.; Wei, Z. P.; Shen, D. Z.; Fan, X. W. *Appl. Phys. Lett.* **2007**, *91*, 021915.
(24) Giles, N. C.; Xu, C. C.; Callahan, M. J.; Wang, B. G.; Neal, J. S.; Boatner, L. A. *Appl. Phys. Lett.* **2006**, *89*, 251906.
(25) Makino, T.; Chia, C. H.; Tuan, N. T.; Segawa, Y.; Kawassaki, M.; Ohtomo, A.; Tamura, K.; Koinuma, H. *Appl. Phys. Lett.* **2000**, *76*, 3549.
(26) Wang, Z. L.; Song, J. H. *Science* **2006**, *14*, 242.
(27) Sela, I.; Smith, D. L. *Phys. Rev. B* **1992**, *46*, 1480.
(28) Rozas, G.; Pascual Winter, M. F.; Fainstein, A.; Jusserand, B.; Vaccaro, P. O.; Saravanan, S. *Phys. Rev. B* **2008**, *77*, 165314.
(29) Cheng, H.-M.; Hsu, H.-C.; Tseng, Y.-K.; Lin, L.-J.; Hsieh, W.-F. *J. Phys. Chem. B* **2005**, *109*, 8749.
(30) Ng, H. T.; Chen, B.; Li, J.; Han, J.; Meyyappan, M. *Appl. Phys. Lett.* **2003**, *82*, 2023.

JP1037975